

A magnetorheological fluid embedded pneumatic vibration isolator allowing independently adjustable stiffness and damping

This article has been downloaded from IOPscience. Please scroll down to see the full text article.

2011 Smart Mater. Struct. 20 085025

(<http://iopscience.iop.org/0964-1726/20/8/085025>)

View [the table of contents for this issue](#), or go to the [journal homepage](#) for more

Download details:

IP Address: 158.132.172.70

The article was downloaded on 09/08/2011 at 01:50

Please note that [terms and conditions apply](#).

A magnetorheological fluid embedded pneumatic vibration isolator allowing independently adjustable stiffness and damping

Xiaocong Zhu, Xingjian Jing¹ and Li Cheng

Department of Mechanical Engineering, Hong Kong Polytechnic University, Hung Hom, Kowloon, Hong Kong, People's Republic of China

E-mail: mmzhuxc@polyu.edu.hk, mmjxj@polyu.edu.hk and mmlcheng@polyu.edu.hk

Received 8 April 2011, in final form 29 June 2011

Published 28 July 2011

Online at stacks.iop.org/SMS/20/085025

Abstract

A magnetorheological (MR) fluid embedded pneumatic vibration isolator (MrEPI) with hybrid and compact connection of pneumatic spring and MR damping elements is proposed in this study. The proposed MrEPI system allows independent nonlinear stiffness and damping control with considerable maneuverable ranges. Meanwhile, it allows convenient switching between different passive and active vibration control modes, thus providing more flexibility and versatility in applications. To demonstrate the advantageous dynamic performance of the MrEPI, a nonlinear non-dimensional dynamic model is developed with full consideration of the nonlinear elements involved. A systematic analysis is therefore conducted which can clearly reveal the influence on system output performance caused by each physically important parameter and provide a useful insight into the analysis and design of nonlinear vibration isolators with pneumatic and MR elements.

(Some figures in this article are in colour only in the electronic version)

1. Introduction

Vibration isolators are extensively used for vibration isolation and suppression [1–6]. Passive isolators can only cover a limited high frequency range and their performance usually deteriorates with changing dynamics. Therefore, active and semi-active vibration isolators have attracted increasing attention.

Various active or semi-active devices have been used in the design of vibration isolators, for example, pneumatic or hydraulic cylinders [7], voice coil motors [8], electromagnetic actuators [9], magnetorheological or electrorheological dampers [10], piezoelectric actuators [11] and intelligent materials such as THUNDER [12] and shape memory alloys [13]. Pneumatic isolators have the advantages of providing high payload, reliable and inexpensive maintenance and low natural frequency, and thus find wide applications

in high precision machinery, measurement apparatus and seismic protection [7, 14]. Usually, a pneumatic isolator with one air chamber cannot provide sufficient damping, which results in excessive vibration around the system's resonance frequency, poor performance at low frequencies, and strongly nonlinear spring dynamics with coupled damping characteristics. To alleviate the problem, some improved structures of pneumatic isolators with passive/active hydraulic and pneumatic damping devices have been developed [15–23]. Although the performance of pneumatic vibration isolation systems can be improved by active damping or optimal design of passive stiffness and damping, the damping introduced by pneumatic orifice valves usually has complex dynamics coupled with the dynamics of the pneumatic chamber and consequently requires complex controller design. Moreover, most systems utilize only one orifice damping device and do not allow independent damping control [6, 18, 24–26].

In a different perspective, magnetorheological (MR) fluids have been extensively used in isolator design as damping-

¹ Author to whom any correspondence should be addressed.

controlled elements [27–32]. MR fluids have several appealing features, i.e., large and controllable dynamic yielding stress due to high magnetic energy density, lower power requirement, robustness against contaminants or impurities and instantaneous response. For decades, vibration isolators consisting of MR dampers and passive spring elements have been developed [3, 21, 33–37]. Most systems are designed to target some specific applications (e.g., shock absorbers [35]), lacking flexibility or adaptability to different situations due to small adjustable range or limited maneuverable variables. Recently, variable stiffness and damping vibration isolators using MR dampers have been studied, in which the stiffness is controlled by one adjustable MR damper and two constant springs in series connection, and the independent variable damping is realized by the other MR damper in parallel [26, 38]. Although these systems allow a simple mechanism to achieve adjustable stiffness, the drawback is linked to the expense and the bulbous structures due to the additional MR dampers and different components involved.

The design of vibration isolators allowing independent adjustment of stiffness and damping is obviously of great relevance in engineering applications since it can provide more flexibility and versatility. However, existing isolator systems, as discussed before, are far from full development.

One potential way to achieve independent adjustment of stiffness and damping is to properly combine the pneumatic spring and MR damping elements in a relatively compact structure. Although conventional single-rod MR dampers have one air chamber to provide the stiffness effect, the gas pressure is either too high for active control, or the system stiffness is too low to effectively support the static load due to the limitation of the effective piston rod area in conventional gas control. Thus, it is important to explore an integrated and more compact structure in using MR fluids and gas to enhance the effective spring and damping characteristics. To this end, an MR fluid embedded pneumatic vibration isolator (MrEPI) is proposed in this study. The MrEPI has a relatively compact structure and can achieve independently adjustable stiffness and damping characteristics of considerable maneuverable ranges. It also provides the flexibility in switching between different working modes (passive, semi-active and active control), has independent height control within a large range, produces high output force, and is convenient in manipulation with lower power requirement.

Note that there are many physical parameters influencing system performance with strongly nonlinear effects in both the pneumatic and MR fluid elements. To demonstrate the advantageous dynamic performance of the MrEPI, a nonlinear non-dimensional dynamic model is systematically developed and analyzed with full consideration of the nonlinear dynamics involved, which is very different from most of the existing results which adopted an approximation to the nonlinearities [34, 39–45]. The nonlinear non-dimensional model can clearly reveal the influence of important physical parameters on system performance and provide a useful insight into the analysis and design of nonlinear vibration isolators with pneumatic and MR elements. It should be noted that

few results are available in the literature regarding the non-dimensional dynamic analysis of MR damping in the context of a vibration isolator system.

The paper is organized as follows. Section 2 gives the structure of the MrEPI using hybrid connection of pneumatic springs and MR dampers. Section 3 presents a non-dimensional dynamic model and analysis for the MrEPI system subject to harmonic excitation. The influences of the non-dimensional physical variables upon system performance are analyzed in section 4. Section 5 details the conclusions drawn.

2. The MrEPI with independently adjustable stiffness and damping

The structure of the proposed MrEPI is shown in figure 1. It consists of three low chambers filled with air (CG1, CG2, CG3) and two upper chambers filled with MR fluid (CM1, CM2). Chamber CG1 and chamber CG2, functioning as a dual-working-chamber pneumatic spring to provide adjustable stiffness and height control, are separated by a moving piston with diaphragm seals and controlled by four pneumatic high speed on–off valves. An auxiliary chamber CG3 is connected to chamber CG2 with a flow restrictor that is designed to operate on a laminar flow region for linear damping. An MR valve is connected to the two sides of a double-rod cylinder filled with MR fluids (chambers CM1 and CM2) to provide adjustable damping. The notable advantages of the MrEPI are summarized as follows.

- (1) Compact structure and convenient realization of active control.

Usually, the effective gas area is determined by the piston rod area in conventional single-rod MR dampers with a small air chamber [30]. To meet a loading requirement, high gas pressure, an additional air spring or a coil spring would be needed [21, 35, 37]. This leads to more mechatronic components involved in the system and thus results in a complex and non-compact system structure. Differently from those designs, the proposed MrEPI employs piston area rather than the conventional piston rod area as the effective area to enlarge the spring force with fewer requirements on volume size. The flow restrictor between chambers CG2 and CG3 can introduce large damping for rejecting a high peak value at resonance frequency and low damping for keeping a fast decaying rate of transmissibility at high frequencies under a small volume for a pneumatic spring with severely nonlinear characteristics.

- (2) Independent adjustable stiffness, damping and height control with large ranges.

The adjustable stiffness can be realized by changing the average pressures of the working gas chambers while keeping a constant pressure difference for invariant static displacement of the isolator owing to the special structure of the dual-working-chamber pneumatic spring. Importantly, the instantaneous stiffness can also be adjusted by changing the gas volume with an additional accumulator [18]. Moreover, the adjustable height of

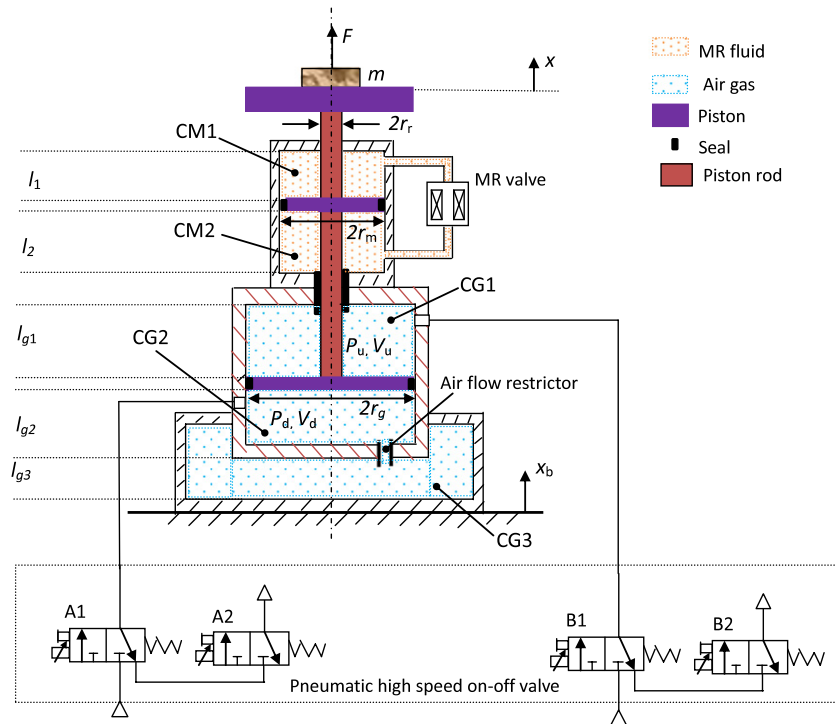


Figure 1. The schematic structure of the MrEPI.

the isolator can be realized by only modifying the pressure difference. Notably, the system damping is independently adjustable through manipulating the field-controlled MR damping element. Therefore, independent stiffness, damping and height control can be realized. This demonstrates a unique system property compared with many existing systems [6, 17–19, 21, 26].

(3) Multiple control modes to improve system flexibility.

The proposed isolator has three operation modes. The passive control mode can be realized by closing valves A1, A2, B1 and B2 to separate the gas chamber from the outside air and setting the MR active damping to zero. This mode is beneficial for vibration isolation at high frequency and invariant working condition [20]. The semi-active control mode can be realized by properly regulating either the pressure of working gas chamber (with on–off valves A1, A2, B1 and B2), the controllable current of the MR damping or the accumulator volume. This mode is beneficial for different requirements under various working conditions within a larger frequency band [25, 26, 36, 46]. The third mode is active control, which can provide arbitrary force through pressure regulation of the pneumatic cylinders. This mode can be used for isolation at ultra-low frequency and complex requirements, such as negative stiffness for rejecting large instantaneous disturbances [4, 14].

(4) Less sealing and power requirements.

Basically, the operating pressure of the MR fluid and pneumatic chamber is lower than that of conventional hydraulic oil. There are no movable components in the MR valve or pneumatic on–off valves utilized in the MrEPI. These designs impose fewer sealing requirements

compared with some existing isolator systems [47–50]. Moreover, in the semi-active control mode, the field-controlled MR valve and on–off pneumatic valves can be employed to control the damping and stiffness characteristics using only a small amount of energy; the power consumption could be much lower compared to a traditional active pneumatic isolator using servo valves [17, 51].

3. Non-dimensional dynamics of the MrEPI

In order to quantitatively analyze and explore the characteristics and potential values of the MrEPI, a non-dimensional dynamic model of the MrEPI is developed in this section. The MrEPI can be considered as three components, i.e., component 1 consisting of pneumatic chamber CG2 and fast switching valves; component 2 consisting of pneumatic chamber CG1 and MR fluid chambers CM1, CM2, and an MR valve; and component 3 consisting of auxiliary chamber CG3 and an air flow restrictor. The equivalent mechanical system of the MrEPI is shown in figure 2 which has a hybrid connection including two pneumatic springs and one passive viscous damper in both serial and parallel, and one MR damper in parallel [18]. Practically, each component can be considered as a sub-isolator with one pneumatic spring and one MR damper. The non-dimensional models of the sub-isolators are first developed, and then the entire non-dimensional model of the MrEPI is obtained by integrating the three sub-models.

3.1. Non-dimensional dynamics of the sub-isolators

The non-dimensional dynamic models of the sub-isolators are developed for the nonlinear pneumatic springs and MR damper

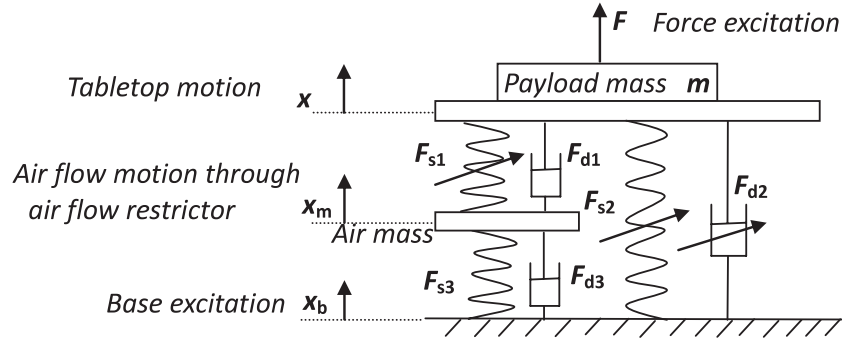


Figure 2. An equivalent mechanical system of the MrEPI system with nonlinear and independent adjustable stiffness and damping characteristics taking an equivalent hybrid connection of each component.

under harmonic excitation by defining some non-dimensional variables.

3.1.1. Output force of the pneumatic spring element. The relationship between the volume and pressure inside the working chambers (CG1 and CG2) can be described by the polytropic gas law [52]

$$P_d \left(\frac{V_d}{m_{ad}} \right)^\lambda = \text{Const}, \quad P_u \left(\frac{V_u}{m_{au}} \right)^\lambda = \text{Const}. \quad (1)$$

If there is no air flowing into or out of the chambers, m_{ad} and m_{au} are constant. Thus the actual gas pressures are given by

$$P_d V_d^\lambda = P_{d0} V_{d0}^\lambda, \quad P_u V_u^\lambda = P_{u0} V_{u0}^\lambda. \quad (2)$$

Note that the initial gas pressure and volume are dependent on the static equilibrium state of the payload, i.e.,

$$A_d P_{d0} - s_u A_u P_{u0} = mg + P_{\text{atm}} A_d - s_u P_{\text{atm}} A_u. \quad (3)$$

For convenience in analysis of the influences due to adjustable pressure, adjustable volume, and variation of the effective area of the pneumatic spring element under certain payload masses, let

$$\begin{aligned} V_{d0} &= V_{dr} + \Delta V_d, & P_{d0} &= P_{dr} + \Delta P_d \\ A_d &= A_{dr} + \Delta A_d \end{aligned} \quad (4)$$

where V_{dr} , P_{dr} , A_{dr} are reference volume, reference pressure and reference effective area, respectively, which satisfy the following static equilibrium state under reference payload mass m_r :

$$m_r g + P_{\text{atm}} A_d - s_u P_{\text{atm}} A_u = P_{dr} A_{dr}. \quad (5)$$

The restoring force (output force) of the pneumatic spring under reference payload is given by

$$\begin{aligned} F_s(x_p) &= A_d(P_d - P_{\text{atm}}) - s_u A_u(P_u - P_{\text{atm}}) - m_r g \\ &= A_d P_d - (m_r g + P_{\text{atm}} A_d) - s_u(P_u - P_{\text{atm}}) A_u \\ &= A_d P_{d0} \left(\frac{V_{d0}}{V_{d0} + A_d x_p} \right)^\lambda - s_u A_u P_{u0} \left(\frac{V_{u0}}{V_{u0} - A_u x_p} \right)^\lambda \\ &\quad - P_{dr} A_{dr} \end{aligned} \quad (6)$$

where $x_p = x - x_b$ is the relative displacement. Let the reference stiffness and initial length be

$$k_0 = \frac{\lambda A_{dr} P_{dr}}{L_0}, \quad (7a)$$

$$L_0 = \frac{V_{dr}}{A_{dr}}. \quad (7b)$$

Substitution of equations (4), (5) and (7) into equation (6) yields

$$\begin{aligned} F_s &= A_{dr} P_{dr} \left\{ (1 + \phi_{P0}) \left(\frac{1}{1 + x_p/L_{d0}} \right)^\lambda \right. \\ &\quad \left. - s_u \phi_{KP} \left(\frac{1}{1 - x_p/L_{u0}} \right)^\lambda - 1 \right\} \\ &= \frac{k_0 L_0}{\lambda} \left\{ (1 + \phi_{P0}) \left(\frac{1}{1 + x_p/L_0(1 + \phi_{V0})} \right)^\lambda \right. \\ &\quad \left. - s_u \phi_{KL} \left(\frac{1}{1 - x_p/\phi_{KL} L_0(1 + \phi_{V0})} \right)^\lambda - 1 \right\} \end{aligned} \quad (8)$$

where ϕ_{V0} , ϕ_{P0} , ϕ_{KP} and ϕ_{KL} are the non-dimensional adjustable variables, which are defined as

$$\phi_{P0} = \frac{\Delta P_d}{P_{dr}} + \frac{\Delta A_d}{A_{dr}} + \frac{\Delta P_d}{P_{dr}} \frac{\Delta A_d}{A_{dr}} \quad (9a)$$

$$\phi_{V0} = \frac{A_{dr}}{A_{dr} + \Delta A_d} \left(\frac{\Delta V_d}{V_{dr}} - \frac{\Delta V_d}{A_{dr}} \right) \quad (9b)$$

$$\phi_{KL} = \frac{L_{u0}}{L_{d0}} \quad (9c)$$

$$\phi_{KP} = \frac{P_{u0} A_u}{P_{dr} A_{dr}} \quad (9d)$$

$$L_{d0} = \frac{V_{d0}}{A_d} \quad (9e)$$

$$L_{u0} = \frac{V_{u0}}{A_u}. \quad (9f)$$

It should be emphasized that the non-dimensional dynamic model in equation (8) of the pneumatic spring element is developed with the nonlinear physical model of the pneumatic isolator system and therefore there is no approximation error due to the linearization that is often used in the literature [39].

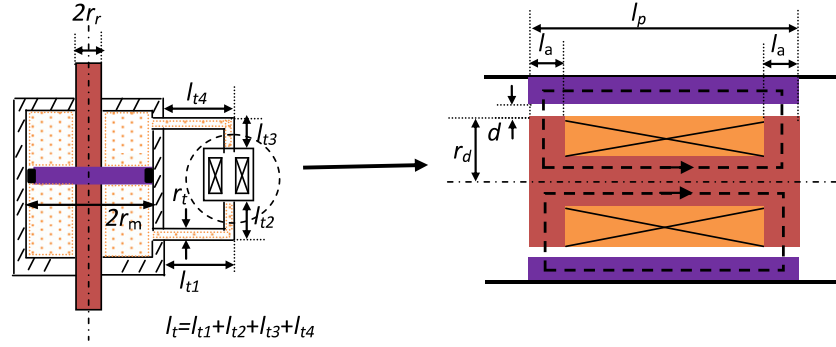


Figure 3. Schematic of the MR fluid cylinder and MR valve.

3.1.2. *Output force of the MR damping element.* The following nonlinear hysteretic model of the MR damping is adopted in our analysis according to the geometric schematics of the MR fluid cylinder and the MR valve shown in figure 3 [27, 53]:

$$F_d(x_p, \dot{x}_p) = c_{vis}\dot{x}_p + (F_\tau + F_f) \tanh\{[(\dot{x}_p + \lambda_1 x_p)]\lambda_2\}. \quad (10)$$

The Newtonian viscous force and yield force due to the MR effect are given by [30, 31, 50]

$$F_\eta = c_{vis}\dot{x}_p \quad (11a)$$

$$F_\tau = \frac{2f_c l_a}{d} \tau_y(H)(A_p - A_{p1}) \quad (11b)$$

where $c_{vis} = (\frac{12\eta l_p}{wd^3} + \frac{8\eta l_t}{\pi r_c^2})(A_p - A_{p1})^2$, and $w = 2\pi(r_d + \frac{d}{2}) \approx 2\pi r_d$, $A_p = \pi r_m^2$, $A_{p1} = \pi r_r^2$. For convenience in analysis, the passive damping is denoted by $F_{dp} = c_{vis}\dot{x}_p$ and the active damping by $F_{da} = (F_\tau + F_f) \tanh\{[(\dot{x}_p + \lambda_1 x_p)]\lambda_2\}$ (although F_{da} usually includes the friction force F_f).

3.1.3. *Non-dimensional dynamics of the sub-isolator under harmonic excitations.* Note that equations (8) and (10) are used to describe the nonlinear spring force and nonlinear damping force with some adjustable design parameters. To assess the influence of design parameters upon isolation performance of the MrEPI, the non-dimensional dynamics under harmonic excitations is established in terms of some deliberately defined non-dimensional variables.

Base excitation. For the sub-isolator in the MrEPI system with pneumatic spring and MR damper elements, merely subjected to a harmonic base excitation (in figure 2, $F = 0$), the equation of motion is given by

$$m\ddot{x} = F_s(x - x_b) - F_d(x - x_b, \dot{x} - \dot{x}_b) \quad (12)$$

$$x_b = \hat{x}_{b0} \sin(\omega t + \varphi)$$

where $F_s(x - x_b)$ and $F_d(x - x_b, (\dot{x} - \dot{x}_b))$ are the spring and damping forces given by equations (8) and (10), respectively.

The dimensions of the variables above can be reduced to three basic dimensions (mass (M), length (L), time (T)). By selecting m , k_0 and \hat{x}_{b0} as the basic independent dimensional

variables, the non-dimensional equation of motion under base excitations can be derived with a reduction method [54]:

$$\frac{d^2\phi_x}{d\phi_t^2} + 2\xi \left(\frac{d\phi_x}{d\phi_t} - \frac{d\Phi_{xb}}{d\phi_t} \right) + 2\xi\phi_{DVMR} \times \tanh\left\{ \left[\left(\frac{d\phi_x}{d\phi_t} - \frac{d\Phi_{xb}}{d\phi_t} \right) + \phi_{\lambda 1}(\phi_x - \Phi_{xb}) \right] \phi_{\lambda 2} \right\} = \frac{\phi_L}{\lambda} \left\{ (1 + \phi_{P0}) \left[\frac{\phi_L(1 + \phi_{V0})}{\phi_L(1 + \phi_{V0}) + \phi_x - \Phi_{xb}} \right]^\lambda - s_u \phi_{KP} \left[\frac{\phi_{KL}\phi_L(1 + \phi_{V0})}{\phi_{KL}\phi_L(1 + \phi_{V0}) - (\phi_x - \Phi_{xb})} \right]^\lambda - 1 \right\} \quad (13)$$

with the normalized base excitation

$$\Phi_{xb} = \sin(\phi_\omega \phi_t + \varphi) \quad \frac{d\Phi_{xb}}{d\phi_t} = \phi_\omega \cos(\phi_\omega \phi_t + \varphi) \quad (14)$$

where ϕ_x , ϕ_ω , ϕ_t are the non-dimensional displacement, frequency and time, respectively. The corresponding non-dimensional variables are defined as

$$L_0 = \phi_L \hat{x}_{b0} \quad (15a)$$

$$c_{vis} = 2\xi \sqrt{mk_0} \quad (15b)$$

$$x = \phi_x \hat{x}_{b0} \quad (15c)$$

$$\phi_{DVMR} = \phi_{DMR} \phi_{VM} \quad (15d)$$

$$\phi_{DVMR} = \frac{F_\tau + F_f}{c_{vis} V_M} \quad (15e)$$

$$\phi_{VM} = \frac{V_M}{\hat{x}_{b0} \omega_n} \quad (15f)$$

$$\lambda_1 = \phi_{\lambda 1} \sqrt{k_0/m} \quad (15g)$$

$$\lambda_2 = \frac{\phi_{\lambda 2}}{\hat{x}_{b0} \sqrt{k_0/m}} \quad (15h)$$

with $t = \phi_t \sqrt{\frac{m}{k_0}}$, $\frac{dx}{dt} = \frac{d\phi_x}{d\phi_t} \hat{x}_{b0} \sqrt{\frac{k_0}{m}}$, $\frac{d^2x}{dt^2} = \frac{d^2\phi_x}{d\phi_t^2} \hat{x}_{b0} \frac{k_0}{m}$, $\omega = \phi_\omega \sqrt{\frac{k_0}{m}}$, $\omega_n = \sqrt{\frac{k_0}{m}} = \frac{\omega}{\phi_\omega}$.

Force excitation. For the sub-isolator in the MrEPI system subjected to merely a harmonic force excitation (in figure 2, $x_b = 0$), the equation of motion is given by

$$m\ddot{x} = F_s(x - x_b) - F_d(x - x_b, \dot{x} - \dot{x}_b) + F$$

$$F = \hat{F}_0 \sin(\omega t + \varphi). \quad (16)$$

By selecting m , k_0 and \hat{F}_0 as the basic independent variables and using the dimension reduction method in [54], the non-dimensional model under force excitation is

$$\frac{d^2\phi_{Fx}}{d\phi_t^2} + 2\xi \frac{d\phi_{Fx}}{d\phi_t} + 2\xi\phi_{FDVMR}$$

$$\times \tanh\left\{\left[\frac{d\phi_{Fx}}{d\phi_t} + \phi_{F\lambda 1}\phi_{Fx}\right]\phi_{F\lambda 2}\right\}$$

$$= \frac{\phi_{FL}}{\lambda} \left\{ (1 + \phi_{P0}) \left[\frac{\phi_{FL}(1 + \phi_{V0})}{\phi_{FL}(1 + \phi_{V0}) + \phi_{Fx}} \right]^\lambda \right.$$

$$\left. - s_u\phi_{KP} \left[\frac{\phi_{KL}\phi_{FL}(1 + \phi_{V0})}{\phi_{KL}\phi_{FL}(1 + \phi_{V0}) - \phi_{Fx}} \right]^\lambda - 1 \right\} + \Phi_F \quad (17)$$

with the normalized force excitation

$$\Phi_F = \sin(\phi_\omega\phi_t + \varphi). \quad (18)$$

The corresponding non-dimensional variables are defined as follows:

$$L_0 = \phi_{FL} \frac{\hat{F}_0}{k_0} \quad (19a)$$

$$x = \phi_{Fx} \frac{\hat{F}_0}{k_0} \quad (19b)$$

$$\phi_{FDVMR} = \phi_{DMR}\phi_{FVM} \quad (19c)$$

$$\phi_{FVM} = \frac{V_M\sqrt{mk_0}}{\hat{F}_0} \quad (19d)$$

$$\lambda_1 = \phi_{F\lambda 1}\sqrt{k_0/m} \quad (19e)$$

$$\lambda_2 = \frac{\phi_{F\lambda 2}\sqrt{k_0m}}{\hat{F}_0} \quad (19f)$$

$$\text{with } \frac{dx}{dt} = \frac{d\phi_{Fx}}{d\phi_t} \frac{\hat{F}_0}{\sqrt{k_0m}}, \quad \frac{d^2x}{dt^2} = \frac{d^2\phi_{Fx}}{d\phi_t^2} \frac{\hat{F}_0}{m}.$$

The force excitation and base excitation can be unified by letting $r_F = \frac{\hat{x}_{b0}k_0}{\hat{F}_0}$. Then

$$\phi_{FL} = r_F\phi_L, \quad \phi_{Fx} = r_F\phi_x, \quad \phi_{FVM} = r_F\phi_{VM},$$

$$\phi_{F\lambda 1} = \phi_{\lambda 1}, \quad \phi_{F\lambda 2} = \frac{\phi_{\lambda 2}}{r_F}.$$

The unified non-dimensional dynamics of the sub-isolator under harmonic excitation is given by

$$\frac{d^2\phi_x}{d^2\phi_t} + F_{dn} \left(\phi_x - \Phi_{xb}, \frac{d\phi_x}{d\phi_t} - \frac{d\Phi_{xb}}{d\phi_t} \right) = F_{sn}(\phi_x - \Phi_{xb}) + \Phi_F \quad (20)$$

where the non-dimensional spring force is given by

$$F_{sn}(\phi_x - \Phi_{xb}) = F_{snb}(\phi_x - \Phi_{xb}) + F_{sna}(\phi_x - \Phi_{xb}) \quad (21a)$$

$$F_{snb}(\phi_x - \Phi_{xb}) = \frac{\phi_L}{\lambda} \left\{ (1 + \phi_{P0}) \right.$$

$$\left. \times \left[\frac{\phi_L(1 + \phi_{V0})}{\phi_L(1 + \phi_{V0}) + (\phi_x - \Phi_{xb})} \right]^\lambda - 1 \right\} \quad (21b)$$

$$F_{sna} = -s_u\phi_{KP} \frac{\phi_L}{\lambda} \left[\frac{\phi_{KL}\phi_L(1 + \phi_{V0})}{\phi_{KL}\phi_L(1 + \phi_{V0}) - (\phi_x - \Phi_{xb})} \right]^\lambda \quad (21c)$$

and the non-dimensional MR damping force is given by

$$F_{dn} = F_{dna} \left(\frac{d\phi_x}{d\phi_t} - \frac{d\Phi_{xb}}{d\phi_t} \right) + F_{dnp} \left(\phi_x - \Phi_{xb}, \frac{d\phi_x}{d\phi_t} - \frac{d\Phi_{xb}}{d\phi_t} \right) \quad (22a)$$

$$F_{dna} = 2\xi\phi_{DVMR} \tanh\left\{\left[\frac{d\phi_x}{d\phi_t} - \frac{d\Phi_{xb}}{d\phi_t} + \phi_{\lambda 1}(\phi_{xp} - \Phi_{xb})\right]\phi_{\lambda 2}\right\} \quad (22b)$$

$$F_{dnp} = 2\xi \left(\frac{d\phi_x}{d\phi_t} - \frac{d\Phi_{xb}}{d\phi_t} \right) \quad (22c)$$

with $\phi_{xp} = \phi_x - \Phi_{xb}$, $\phi_L = \frac{L_0}{x_{b0}}$ for base excitation, and $\phi_L = \frac{L_0k_0}{F_0}$ for force excitation.

Static equilibrium state of the vibration isolator. According to equations (20)–(22), the static equilibrium state is given by

$$(1 + \phi_{P0}) \left[\frac{1}{1 + \phi_{x0}/[\phi_L(1 + \phi_{V0})]} \right]^\lambda$$

$$- s_u\phi_{KP} \left[\frac{1}{1 - \phi_{x0}/[\phi_{KL}\phi_L(1 + \phi_{V0})]} \right]^\lambda = 1. \quad (23)$$

For a single-working-chamber pneumatic spring ($s_u = 0$ in equation (23)), the static displacement could be adjusted by pressure regulation, i.e., by changing the additional pressure ratio ϕ_{P0} . From equation (23),

$$(1 + \phi_{P0}) \left[\frac{\phi_L(1 + \phi_{V0})}{\phi_L(1 + \phi_{V0}) + \phi_{x0}} \right] = 1. \quad (24)$$

Thus, the static displacement is given by

$$\phi_{x0} = [(1 + \phi_{P0})^{1/\lambda} - 1]\phi_L(1 + \phi_{V0}). \quad (25)$$

It is noted that the variation of ϕ_{P0} is equivalent to the variation of ϕ_{V0} , which satisfies

$$\phi'_{V0} = [(1 + \phi_{P0})^{1/\lambda} - 1]. \quad (26)$$

For a dual-working-chamber pneumatic spring ($s_u = 1$ in (23)), zero static displacement of the isolator could also be obtained if $\phi_{P0} = \phi_{KP}$ (see equation (23)). This means that the stiffness of the dual-working-chamber pneumatic spring could be adjusted by pressure regulations without height variation.

3.2. Non-dimensional dynamics of the MrEPI system

Similarly to equation (20), the non-dimensional dynamics of the MrEPI in hybrid connection with three sub-isolators

characterized by equations (21) and (22) is consequently given by

$$\begin{aligned} \frac{d^2\phi_x}{d\phi_t^2} &= F_{sn1}(\phi_x - \phi_{xm}) - F_{dn1}\left(\phi_x - \phi_{xm}, \frac{d\phi_x}{d\phi_t} - \frac{d\phi_{xm}}{d\phi_t}\right) \\ &+ F_{sn2}(\phi_x - \Phi_{xb}) - F_{dn2}\left(\phi_x - \Phi_{xb}, \frac{d\phi_x}{d\phi_t} - \frac{d\Phi_{xb}}{d\phi_t}\right) + \Phi_F \\ &F_{sn1}(\phi_x - \phi_{xm}) - F_{dn1}\left(\phi_x - \phi_{xm}, \frac{d\phi_x}{d\phi_t} - \frac{d\phi_{xm}}{d\phi_t}\right) \\ &= F_{sn3}(\phi_{xm} - \Phi_{xb}) - F_{dn3}\left(\phi_{xm} - \Phi_{xb}, \frac{d\phi_{xm}}{d\phi_t} - \frac{d\Phi_{xb}}{d\phi_t}\right) \end{aligned} \quad (27)$$

where F_{sn1} and F_{dn1} are the spring and damping forces of the pneumatic spring due to low chamber CG2; F_{sn3} and F_{dn3} are the spring and damping forces of the pneumatic spring due to the auxiliary chamber and air restrictor; and F_{sn2} and F_{dn2} are the spring and damping forces of the pneumatic spring due to the upper chamber CG1 and the MR damping element. The parameter r_p ($0 \leq r_p \leq 1$) is a parallel ratio which is to guarantee invariant static displacement in the case of parallel connections. The parameter ϕ_{xm} is the displacement of the middle platform in series connection.

Although there are contributions from the pneumatic spring as a damping force (i.e., F_{dn1}) or from the MR damper as a spring force, these forces have no coupling effects with the corresponding main damping and spring forces F_{dn2} , F_{sn1} and F_{sn2} , and can basically be neglected compared with the main factors due to the inherent structure of the MrEPI. Similar cases hold for F_{sn3} and F_{dn3} . Note also that the spring forces F_{sn1} and F_{sn2} from the pneumatic springs are nonlinear functions of the parameters ϕ_{P0} and ϕ_{V0} respectively, and the damping force F_{dn2} from the MR damper is a nonlinear function of the parameter ϕ_{DVMR} . No coupling exists among these critical parameters either. Therefore, the overall stiffness and damping can be independently controlled to any values by the pneumatic spring element and the MR damper element, respectively. Practically, ϕ_{V0} , ϕ_{P0} and ϕ_{DVMR} can be used to control independently the spring force F_{s1} , the spring force F_{s2} and the damping force F_{d2} , respectively.

3.3. Model verification

To verify the non-dimensional dynamic model established above, the transmissibility of the non-dimensional model and the actual plant dynamic model of the MrEPI can be compared. To this end, the linearized non-dimensional models of the pneumatic springs and MR damper can be derived through the first-order Taylor series expansion for equation (21) and Fourier transform for equation (22) as in [42], i.e.,

$$F_{snl} = -K_n \phi_{xp} \quad (28a)$$

$$F_{dnl} = (2\xi + 2\xi_a) \frac{d\phi_{xp}}{d\phi_t} \quad (28b)$$

where $K_n = K_{an} + K_{bn}$, $K_{an} = \frac{s_u \phi_{KP}}{\phi_{KL}(1+\phi_{V0})}$, $K_{bn} = \frac{1+\phi_{P0}}{1+\phi_{V0}}$, $\xi_a = \int_0^{2\pi/\phi_\omega} F_{nda} \phi_\omega \cos(\phi_\omega \phi_t) d\phi_t / 2\pi \phi_\omega$. Substituting equation (28) into equation (27), the transmissibility of the

non-dimensional model of the MrEPI in figure 2 could be obtained through the Laplace transform of equation (27) as

$$\frac{\phi_x(s)}{\Phi_{xb}(s)} = \frac{K_n^* + (2\xi_2 + 2\xi_{a2})s}{s^2 + K_n^* + (2\xi_2 + 2\xi_{a2})s} \quad (29)$$

where $K_n^* = \frac{1}{1/[K_{n1} + (2\xi_1 + 2\xi_{a1})s] + 1/[K_{n3} + (2\xi_3 + 2\xi_{a3})s]} + K_{n2}$.

On the other hand, the actual plant of the MrEPI in figure 1 is given by [16, 52]

$$\begin{aligned} \dot{P}_u &= \frac{\lambda RT_u Q_{mu}}{V_u} - \frac{\lambda P_u \dot{V}_u}{V_u} \\ \dot{P}_d &= \frac{\lambda RT_d Q_{md}}{V_d} - \frac{\lambda P_u \dot{V}_d}{V_d} - \frac{\lambda RT_d Q_{mc}}{V_d} \\ \dot{P}_c &= \frac{\lambda RT_c Q_{mc}}{V_c} \end{aligned}$$

$$m\ddot{x} = (P_d - P_{atm})A_d - s_u(P_u - P_{atm})A_u - mg - F_d + F \quad (30)$$

where $Q_{mc} = C_r \rho (P_d - P_c)$ is the laminar flow rate due to the air flow restrictor; $\rho = \frac{P_d + P_c}{2RT_c}$; $C_r = \frac{\pi d^4}{128\mu L}$; and $Q_{mu} = Q_{md} = 0$ for the passive mode. For comparison, equation (30) can also be linearized through the Taylor series expansion in the neighborhood of the static equilibrium point with initial states $P_{c0} = P_{d0}$, $T_{a0} = T_{d0} = T_{c0} = T_0$ and applying Fourier transform for the active damping part of the MR damper:

$$\begin{aligned} \dot{P}_u &= \frac{\lambda P_{u0} A_u \dot{x}_p}{V_{u0}} \\ \dot{P}_d &= -\frac{\lambda P_{d0} A_d \dot{x}_p}{V_{d0}} - \frac{V_{c0} \dot{P}_c}{V_{d0}} \\ \dot{P}_c &= R_F (P_d - P_c) \end{aligned} \quad (31)$$

$$m\ddot{x} = \dot{P}_d A_d - s_u \dot{P}_u A_u - (c_{vis} + c_a) \dot{x}$$

where $R_F = \frac{\lambda C_r P_{a0}}{V_{c0}}$, $c_a = \int_0^{2\pi/\omega} F_{da} \hat{x}_{b0} \omega \cos(\omega t) dt / \pi \omega \hat{x}_{b0}^2$. Therefore, the transmissibility of the actual plant dynamics of the MrEPI could be given by

$$\frac{x(s)}{x_b(s)} = \frac{K^* + (c_{vis} + c_a)s}{ms^2 + K^* + (c_{vis} + c_a)s} \quad (32)$$

where $K^* = \frac{1}{\frac{1}{K_d} + \frac{1}{K_c(s/R_F + 1)}} + s_u K_u$, $K_d = \frac{\lambda P_{d0} A_d^2}{V_{d0}}$, $K_c = \frac{\lambda P_{c0} A_c^2}{V_{c0}}$, $K_u = \frac{\lambda P_{u0} A_u^2}{V_{u0}}$. According to equations (7), (9), (15) and (29), equation (32) can be rewritten as

$$\begin{aligned} \frac{x(s)}{x_b(s)} &= \frac{k_0 K_n^* + \sqrt{mk_0}(2\xi + 2\xi_a)s}{ms^2 + k_0 K_n^* + \sqrt{mk_0}(2\xi + 2\xi_a)s} \\ &= \frac{2\xi_p \omega_p s + \omega_p^2}{s^2 + 2\xi_p \omega_p s + \omega_p^2} \end{aligned} \quad (33)$$

where $\omega_p = \sqrt{\frac{k_0}{m} \sqrt{K_n^*}}$, $\xi_p = \frac{\xi + \xi_a}{\sqrt{K_n^*}}$, and the appropriate non-dimensional values for the three components in equation (29) are set as $K_{bn1} = \frac{K_d}{k_0} = \frac{1+\phi_{P0}}{k_0(1+\phi_{V0})}$, $K_{an2} = \frac{K_u}{k_0} = \frac{\phi_{KP2}}{k_0 \phi_{KL2}(1+\phi_{V02})}$,

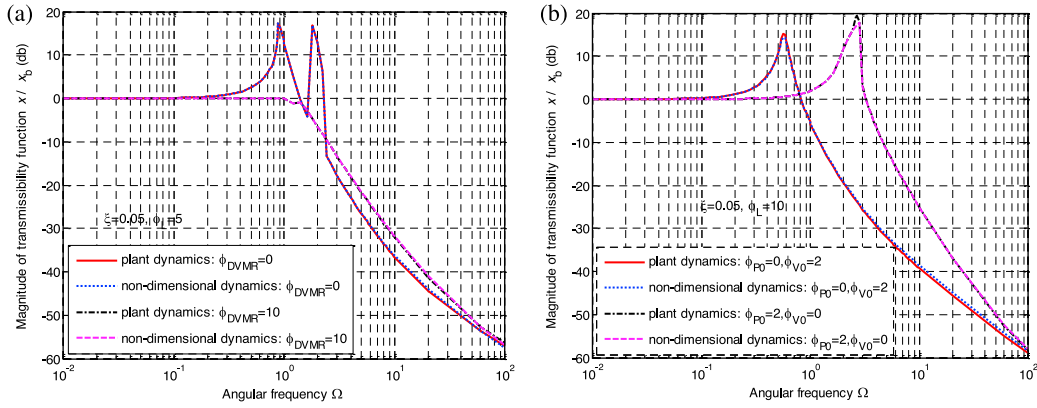


Figure 4. Transmissibility comparison of non-dimensional dynamics and actual plant dynamics of the MrEPI. (a) Transmissibility under different ϕ_{DVMR} . (b) Transmissibility under different ϕ_{P0} and ϕ_{V0} .

$$K_{bn3} = \frac{K_c}{k_0} = \frac{1 + \phi_{P03}}{k_0(1 + \phi_{V03})}, \quad K_{an1} = K_{bn2} = K_{an3} = 0, \\ \xi_1 = \xi_{a1} = \xi_{a3} = 0, \quad \xi_2 = \xi, \quad \xi_{a2} = \xi_a, \quad \xi_3 = \frac{K_{bn3}}{2R_F \sqrt{mk_0}}$$

Therefore, the non-dimensional dynamics of the MrEPI is basically equivalent to the actual plant dynamics. That is, the non-dimensional dynamics provides a convenient insight into the quantitative analysis and design for the MrEPI with normalized formulation regardless of the different load mass and stiffness configuration that exists for the actual plant system.

For further verification, the simulation results using the nonlinear non-dimensional model of the MrEPI under different parameter values and the actual model with physical parameters calculated by equations (7), (9), (15) and (19) are given in figure 4, where the x -axis for the actual plant dynamics uses normalized frequency. Almost no differences between the transmissibilities of the two dynamic models (non-dimensional and actual ones) are observed for any non-dimensional variables. Moreover, the natural frequency for $\phi_{V0} = 2$ is $\omega_p = 0.563$, which is approximately consistent with the theoretical calculation using equation (33) ($\omega_p = \sqrt{1/(1 + \phi_{V0})} = 0.578$) (see figure 4(b)). Thus the non-dimensional model established is effective for the analysis and design of nonlinear vibration isolators consisting of pneumatic springs and MR dampers.

4. Performance evaluation of the MrEPI through simulation

Using equation (27), the influences of non-dimensional variables on system performance could be quantified to provide a clear understanding of the dynamic characteristics and structural design of the MrEPI. The default values of the non-dimensional variables used are listed in table A.1 (see appendix).

4.1. Performance index of the vibration isolator

To evaluate the isolation performance of a vibration isolator, there are usually two performance indices for the linear vibration isolation system (displacement transmissibility and force mobility) [39]. However, in nonlinear isolators the

transmitted signal may contain subharmonics, superharmonics, and sometimes chaotic behaviors. Therefore, the generalized transmissibility and the force mobility are adopted [55]

$$TR = \frac{\sqrt{E[(x - \bar{x})^2]}}{\sqrt{E[(x_b - \bar{x}_b)^2]}}, \quad (34a)$$

$$TF = \frac{\sqrt{E[(\dot{x} - \bar{\dot{x}})^2]}}{\sqrt{E[(F - \bar{F})^2]}} \quad (34b)$$

where \bar{x} , $\bar{\dot{x}}$, \bar{x}_b and \bar{F} are mean values of x , \dot{x} , x_b and F , and $E[\cdot]$ is to take the mean value of a variable in steady state response.

4.2. Effects of different variables on the pneumatic spring dynamics

The design parameters of the pneumatic spring element include ϕ_L , λ , ϕ_{P0} , ϕ_{V0} , ϕ_{KP} and ϕ_{KL} . In view of the symmetric excitation, ϕ_{KL} is set to 1 without imposing restrictions. Since the polytropic exponent λ is included in the definition of reference stiffness (equation (7a)) and also the non-dimensional model is not affected by the payload and reference stiffness, the influence of λ is omitted. Note that the pneumatic spring is nonlinear and the stiffness of the isolator can be easily adjusted via the pressure and volume. Therefore, the influences upon the isolation performance incurred by the nonlinearity degree ratio ϕ_L , additional volume ratio ϕ_{V0} and additional pressure ratio ϕ_{P0} along with ϕ_{KP} are investigated in this section.

4.2.1. Influence of the nonlinearity degree ratio ϕ_L . The dynamics of the isolator with small and large damping under different nonlinearity degree ratios ϕ_L are given in figures 5 and 6.

In figures 5(a) and 6(a), the peak value at linear resonance frequency $\Omega = 1$ decreases when ϕ_L is set smaller. However, there is a fairly large peak at the harmonic frequency when ϕ_L and damping ξ are both set smaller. In figures 5(b) and 6(b), the generalized force mobility usually has its peak value at the linear resonance frequency, which is reduced with larger damping value and smaller ϕ_L . However, there

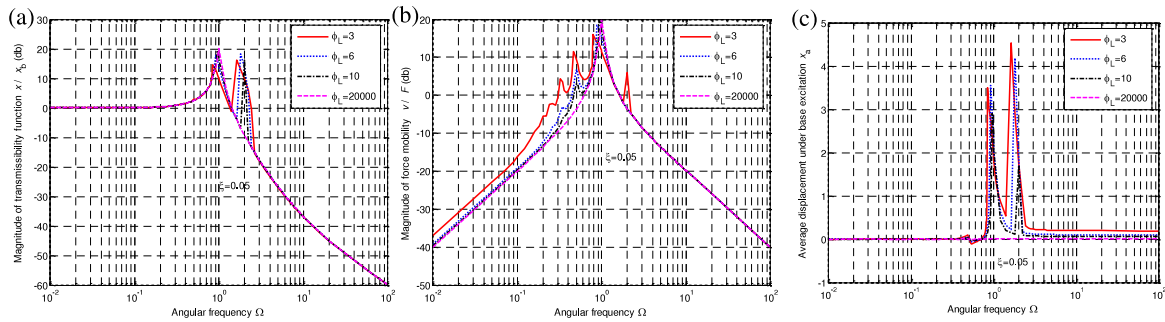


Figure 5. Isolation performance with small damping under different nonlinearity degree ratios ϕ_L . (a) Generalized transmissibility under base excitation. (b) Force mobility function under force excitation. (c) Average displacement under base excitation.

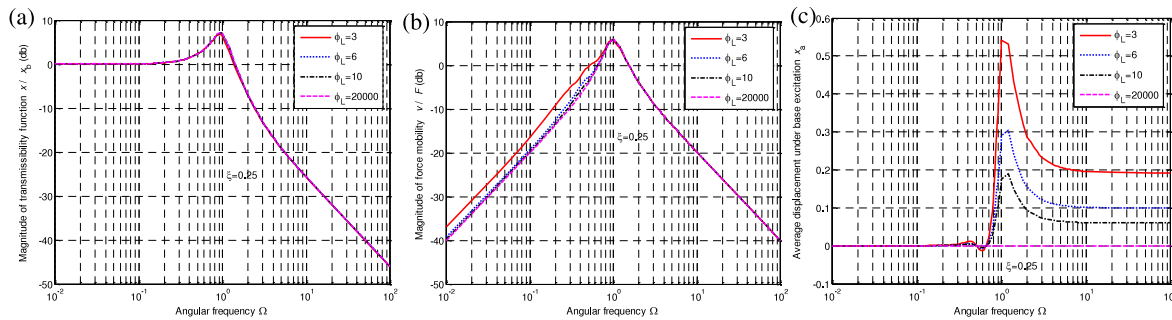


Figure 6. Isolation performance with large damping under different nonlinearity degree ratios ϕ_L . (a) Generalized transmissibility under base excitation. (b) Force mobility function under force excitation. (c) Average displacement under base excitation.

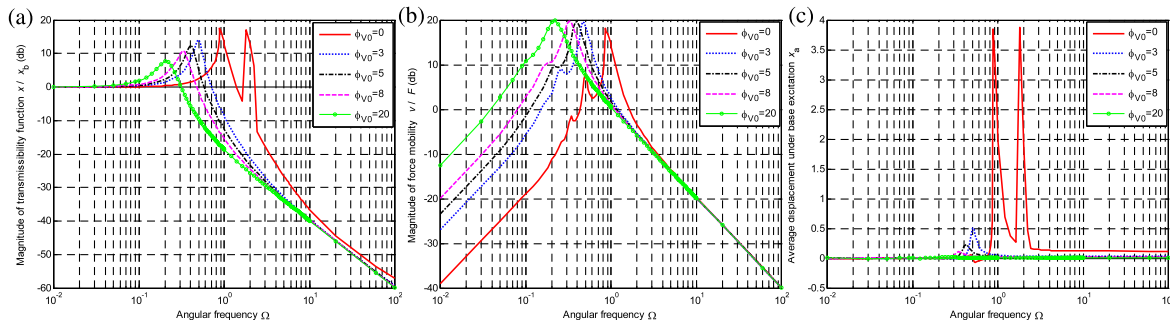


Figure 7. Isolation performance under different additional volume ratios ϕ_{V0} . (a) Generalized transmissibility under base excitation. (b) Force mobility function under force excitation. (c) Average displacement under base excitation.

are multiple peaks below the linear resonance frequency. The system demonstrates obvious subharmonics in force mobility and superharmonics in transmissibility because of the nonlinear pneumatic spring. This could bring difficulties in low frequency vibration control. Another nonlinear behavior is that the average displacement under base excitation is zero at low frequency and increases greatly around the linear resonance frequency, and consequently maintains a small static displacement at high frequency (see figures 5(c) and 6(c)). Note that ϕ_L represents the degree of nonlinearity of the pneumatic spring. Therefore, a larger excitation amplitude or smaller initial length results in more complicated nonlinear dynamics of the pneumatic spring under a small damping effect, and the nonlinear dynamics brings a smaller peak value at the linear resonance frequency, obvious superharmonics in transmissibility and subharmonics in force mobility as well as larger nonzero average displacement at high frequency.

4.2.2. *Influence of the additional volume ratio ϕ_{V0} .* The effects of the additional volume ratio ϕ_{V0} are shown in figure 7. All the nonlinear characteristics including superharmonics, subharmonics and the nonzero average displacement at high frequency observed in the previous cases tend to disappear while the force mobility at low frequency deteriorates when ϕ_{V0} is set larger. This demonstrates the effect of the additional air volume in counteracting the nonlinear effects in the system. Moreover, both the first peak value of transmissibility and the resonance frequency decrease when ϕ_{V0} is set larger, indicating that the natural frequency and stiffness of the isolator can be adjusted by ϕ_{V0} . Therefore, a larger additional volume is helpful to remove the nonlinear effects in the pneumatic spring and result in a smaller stiffness of the isolator with smaller transmissibility peak but poor capability in rejecting force disturbance around the resonance frequency.

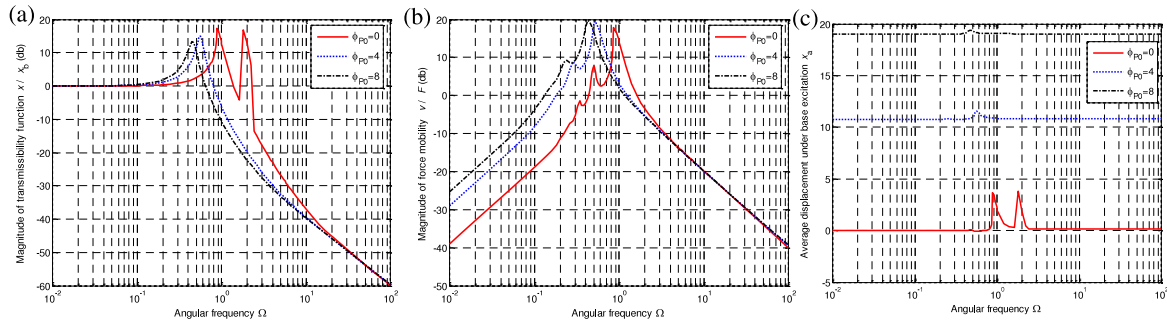


Figure 8. Isolation performance under different additional pressure ratios ϕ_{P0} for the single-working-chamber pneumatic spring. (a) Generalized transmissibility under base excitation. (b) Force mobility function under force excitation. (c) Average displacement under base excitation.

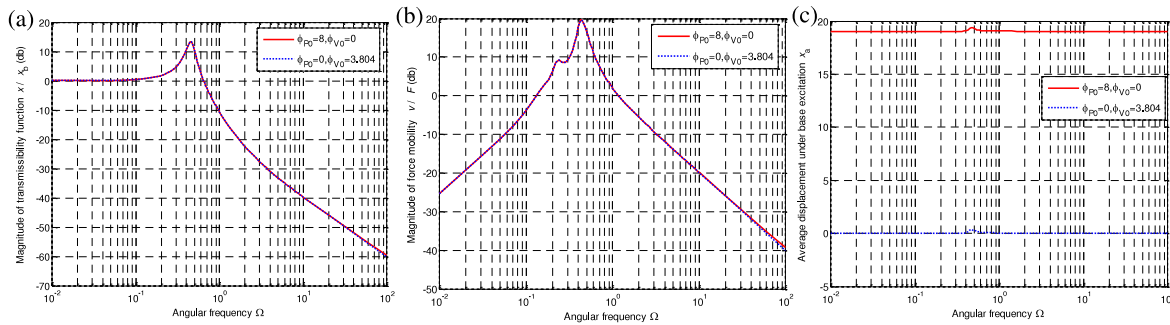


Figure 9. Performance under additional pressure ratio ϕ_{P0} and its equivalent additional volume ratio ϕ_{V0} for the single-working-chamber pneumatic spring. (a) Generalized transmissibility under base excitation. (b) Force mobility function under force excitation. (c) Average displacement under base excitation.

4.2.3. Influence of the additional pressure ratio ϕ_{P0} . The influence of the additional pressure ratio ϕ_{P0} for the single-working-chamber pneumatic spring (i.e., $s_u = 0$) is shown in figure 8, where the resonance frequency, peak value of transmissibility, magnitude of force mobility and static displacement of the isolator are adjustable through manipulating ϕ_{P0} . The system tends to be more linear with weak superharmonics in transmissibility and weak subharmonics in force mobility, and also demonstrates smaller stiffness and poor capability of rejecting force disturbance at around the resonant frequency when ϕ_{P0} is set larger. Since ϕ_{P0} is related to the additional pressure of the pneumatic spring, it can be concluded that large static displacement, more linear behavior and small stiffness of the isolator can be achieved by utilizing a large difference between the additional pressure and the reference pressure for the single-working-chamber pneumatic spring.

Actually, the two parameters ϕ_{P0} (additional pressure) and ϕ_{V0} (additional volume) have the same effects of transmissibility and force mobility in the entire frequency band (figures 9(a) and (b)) but different height effects (figure 9(c)). Figure 9 shows the frequency responses under different ϕ_{P0} and equivalent ϕ_{V0} for the single-working-chamber pneumatic spring. Variation of the additional volume can achieve adjustable instantaneous stiffness while variation of the additional pressure can be employed to adjust the height of the isolator, which is consistent with suggestions in [17].

For the dual-working-chamber pneumatic spring case (i.e., $s_u = 1$), the system stiffness can also be changed by adjusting

the additional pressure ratio while the static displacement can always be guaranteed to be zero when $\phi_{KP} = \phi_{P0}$. In figure 10, the system resonance frequency is increased and the magnitude of the force mobility is decreased when ϕ_{P0} is increased while keeping $\phi_{KP} = \phi_{P0}$. This indicates that the system stiffness and capability in rejecting force disturbance are increased. The static displacement under low frequencies is always zero due to the invariant static equilibrium when $\phi_{KP} = \phi_{P0}$. Thus stiffness adjustment with invariant static displacement of the isolator can be achieved by changing the difference between the additional pressure and the reference pressure while keeping the pressure ratio of the dual-working-chamber pneumatic spring equal to the additional pressure ratio.

4.3. Effects of different variables on the MR damping dynamics

The main design parameters of the MR damping element are ξ , ϕ_{DVMR} , $\phi_{\lambda 1}$ and $\phi_{\lambda 2}$, the influences of which are analyzed in this section.

4.3.1. Influence of the dynamic range of the MR active damping ϕ_{DVMR} .

The system response under different ϕ_{DVMR} is shown in figure 11. The peak value of transmissibility at the resonance frequency and the maximum average displacement under base excitation are decreased greatly when ϕ_{DVMR} increases. Moreover, the magnitude of force mobility is small and nearly

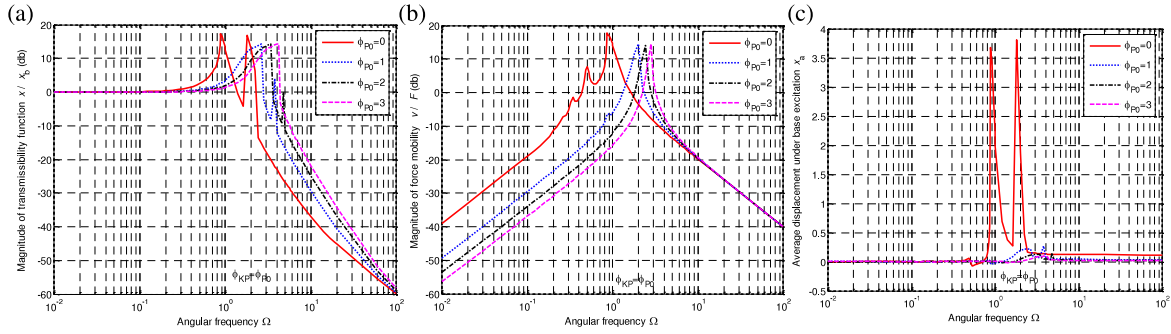


Figure 10. Isolation performance under different additional pressure ratios ϕ_{P0} for the dual-working-chamber pneumatic spring. (a) Generalized transmissibility under base excitation. (b) Force mobility function under force excitation. (c) Average displacement under base excitation.

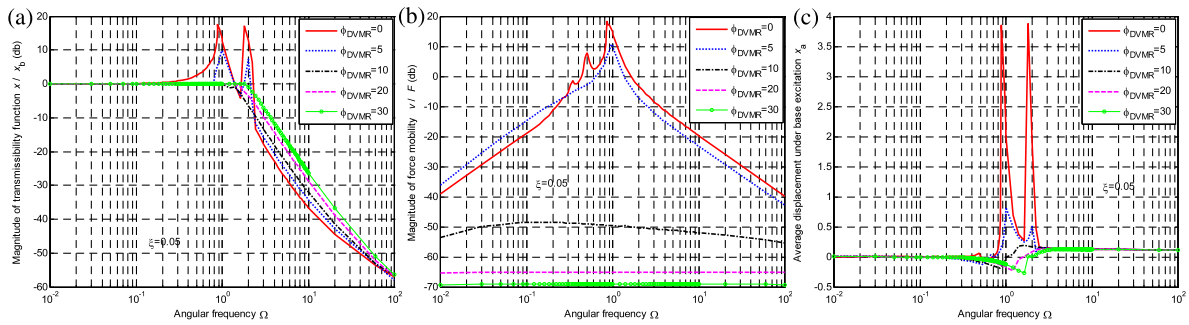


Figure 11. Isolation performance under different dynamic ranges of the MR active damping ϕ_{DVMR} . (a) Generalized transmissibility under base excitation. (b) Force mobility function under force excitation. (c) Average displacement under base excitation.

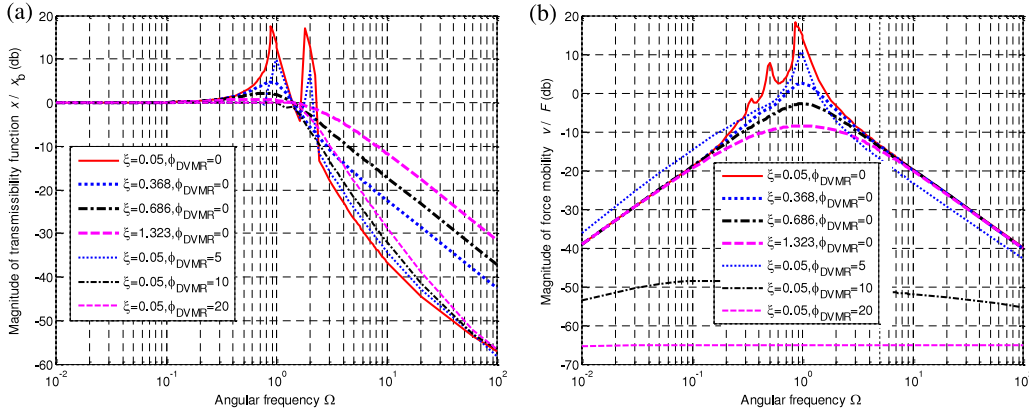


Figure 12. Isolation performance under different dynamic ranges of the MR active damping and the equivalent viscous damping. The equivalent viscous damping is 0.368 when the MR damping $\phi_{DVMR} = 5$ and $\xi = 0.05$, it is 0.686 when $\phi_{DVMR} = 10$ and $\xi = 0.05$, and it is 1.323 when $\phi_{DVMR} = 20$ and $\xi = 0.05$. (a) Generalized transmissibility under base excitation. (b) Force mobility function under force excitation.

constant under large ϕ_{DVMR} at all frequencies, indicating the excellent capability of resisting force disturbance over all frequency bands. Note that a larger ϕ_{DVMR} implies a larger available nonlinear active damping. Therefore, the capability of resonance attenuation under base excitation and disturbance rejection under force excitation can generally be significantly improved by increasing the nonlinear damping effect.

To further evaluate the nonlinear damping characteristics of the MR damping, the isolation performances under different dynamic ranges of ϕ_{DVMR} and the equivalent viscous damping

[53] at the natural frequency $\Omega = 1$ are shown in figure 12. It is noted that the nonlinear damping has a smaller peak value at the resonance frequency and a faster decaying rate at high frequencies than those of the constant equivalent viscous damping, indicating the advantageous characteristics of nonlinear damping [56].

4.3.2. Influence of the hysteretic width coefficient $\phi_{\lambda 1}$. The comparison under different hysteresis width coefficients $\phi_{\lambda 1}$ is shown in figure 13. The transmissibility at resonance

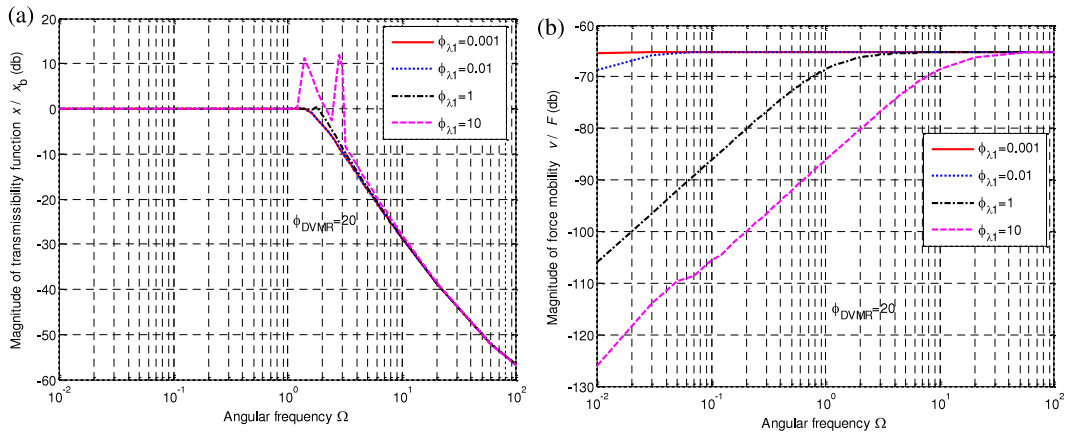


Figure 13. Isolation performance under different hysteresis width coefficients $\phi_{\lambda 1}$. (a) Generalized transmissibility under base excitation. (b) Force mobility function under force excitation.

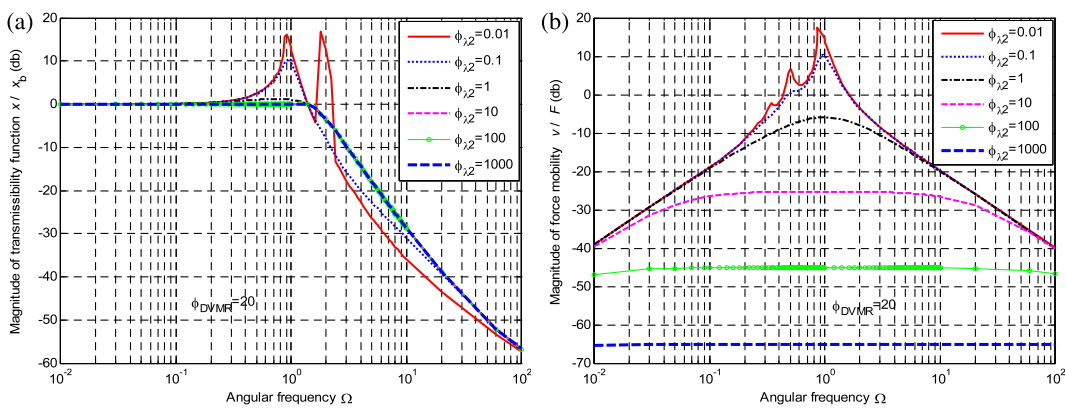


Figure 14. Isolation performance under different velocity-dependent hysteresis coefficients $\phi_{\lambda 2}$. (a) Generalized transmissibility under base excitation. (b) Force mobility function under force excitation.

frequency decreases while the force mobility at low frequencies increases with $\phi_{\lambda 1}$ increasing. The decaying rate of transmissibility at high frequency is only slightly affected by $\phi_{\lambda 1}$. This is also the case for the transmissibility performance when $\phi_{\lambda 1}$ is small (e.g., $\phi_{\lambda 1} < 0.01$). Thus, a large hysteresis width of the MR damping force (i.e., severe displacement-dependent hysteresis) results in a smaller damping effect under base excitation and a greater damping effect under force excitation at low frequencies, while better resonance attenuation and disturbance rejection as well as a faster decaying rate at high frequency may be achieved with a smaller hysteresis width.

4.3.3. Influence of the hysteretic slope coefficient $\phi_{\lambda 2}$. The isolation performance under different hysteresis slope coefficients $\phi_{\lambda 2}$ is shown in figure 14. A smaller transmissibility peak at the resonance frequency and nearly constant force mobility magnitude at all frequencies are achieved and the nonlinear damping effect becomes more dominant, when $\phi_{\lambda 2}$ is increased. When $\phi_{\lambda 2}$ is too large (e.g., $\phi_{\lambda 2} > 100$), the transmissibility performance is only slightly influenced by $\phi_{\lambda 2}$. Therefore, a larger hysteresis slope introduces a more effective velocity-dependent

nonlinear damping force, which is helpful to attenuate the transmissibility peak and resist force disturbance.

4.4. Effects of the passive damping of the auxiliary chamber

In application, the volume of the gas chamber should be as small as possible to achieve compact structure and reduced cost. The variable ϕ_{V0} is a useful design parameter to evaluate the required gas volume. The same gas volume could be obtained for a difference of 1 between the additional volume ratios in parallel connection (i.e., the isolator without auxiliary chamber, a special case of the MrEPI with $\xi_3 = 0$) and in hybrid connection (i.e., the isolator with auxiliary chamber and restrictor connecting to the working chamber, the proposed case for the MrEPI with $\xi_3 > 0$) under the same nonlinearity degree ratio. The comparisons between hybrid and parallel connections under the same volume constraint but different passive damping of the restrictor are shown in figure 15. The hybrid connection can achieve a much smaller transmissibility peak value and better force mobility as well as a small maximum average displacement around the resonance frequency under both small and large passive damping of the restrictor ξ_3 . The larger ξ_3 is, the smaller the transmissibility peak value and force mobility that can

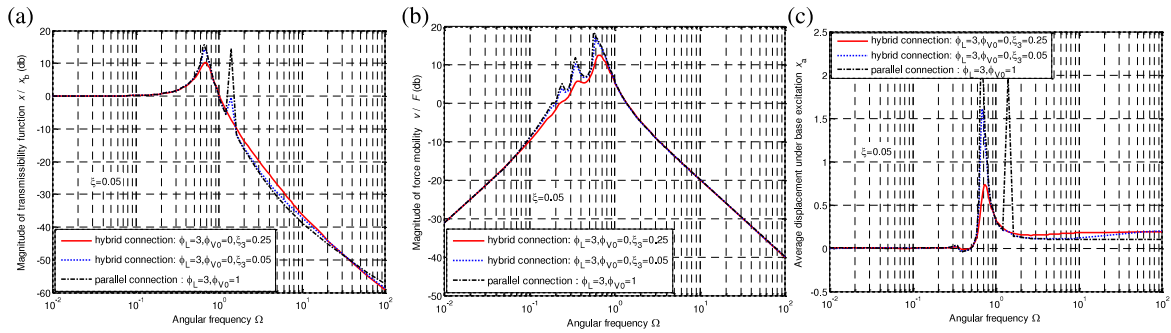


Figure 15. Isolation performance of the hybrid and parallel connections under the same volume constraint as well as different passive dampings of the restricter. (a) Generalized transmissibility under base excitation. (b) Force mobility function under force excitation. (c) Average displacement under base excitation

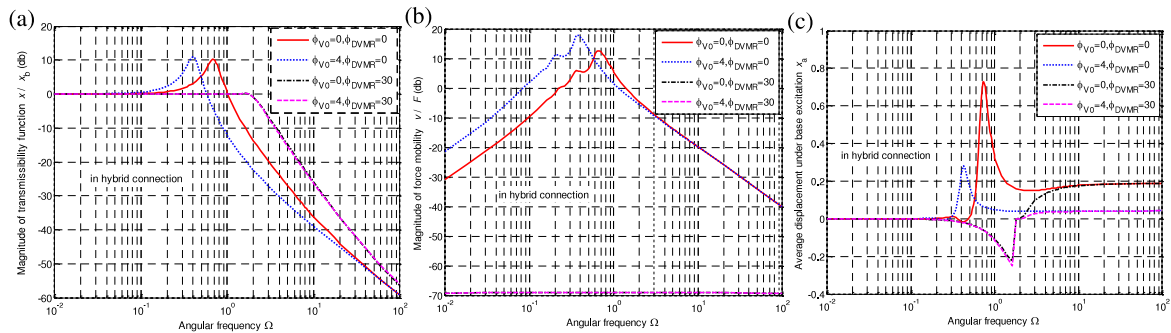


Figure 16. Isolation performance of the MrEPI under different additional volume ratios ϕ_{V0} and MR active dampings ϕ_{DVMR} . (a) Generalized transmissibility under base excitation. (b) Force mobility function under force excitation. (c) Average displacement under base excitation.

be obtained are. Thus, the isolator in hybrid connection can achieve better performance under the same volume constraint compared to the isolator in pure parallel connection of the pneumatic spring and damping element.

4.5. Performance of the MrEPI with independent stiffness and damping control

The achievable isolation performance of the MrEPI with independent stiffness and damping control could be evaluated through the three adjustable non-dimensional variables, i.e., the additional volume ratio ϕ_{V0} , the additional pressure ratio ϕ_{P0} and the dynamic range of the MR active damping ϕ_{DVMR} . The adjustable range is between 0 and 4 for ϕ_{V0} , between 0 and 3 for ϕ_{P0} , and between 0 and 30 for ϕ_{DVMR} . The other parameters in the simulation are $\phi_L = 3$, $\xi_1 = 0.005$, $\xi_2 = 0.05$ and $\xi_3 = 0.25$. It should be noted that the system resonance frequency is usually around the natural frequency, and the latter is dependent on the stiffness of the passive isolator. Therefore, the stiffness under certain additional pressure or additional volume values can basically be evaluated by the resonance frequency that can be seen from the transmissibility function in the following sections.

4.5.1. Achievable performance through adjusting the additional volume and MR active damping. Figure 16 shows the performance of the MrEPI under adjustable additional volume ratio ϕ_{V0} and dynamic range of the MR active damping

ϕ_{DVMR} , where ϕ_{V0} is used to adjust the stiffness of the isolator and ϕ_{DVMR} is used to adjust the damping. The achievable performance is evaluated in table 1 and the corresponding performances for parallel and series connections of the spring and damper elements are also given for comparison, which show that the performance of the hybrid structure is basically better than the others in terms of the achievable stiffness and peak values. The stiffness of the hybrid isolator could be adjusted within 0.4 and 0.68 by the additional volume. Note that the range for ϕ_{V0} is restricted to [0 4] for all the cases in the comparisons, and actually larger ϕ_{V0} results in even smaller stiffness. In application, the stiffness could be designed to reject low frequency or static force disturbance since the magnitude of the force mobility at low frequency is greatly influenced by the adjustable stiffness (see figure 16(b)). On the other hand, the transmissibility peak value and decaying rate at high frequency can both be modified obviously with different damping effects to attenuate vibration under certain stiffnesses (figure 16(a)), with simultaneously rejecting force disturbance at all frequencies (figure 16(b)). Moreover, a smaller maximum average displacement around the resonance frequency under force and base excitations could be achieved, as seen from table 1 and figure 16(c). Thus, the isolation performances, including zero peak value and fairly small magnitude of the force mobility at low frequencies, and fast decaying rate of transmissibility at high frequencies under certain stiffnesses, could all be achieved simultaneously by the MrEPI due to the independently adjustable stiffness and damping.

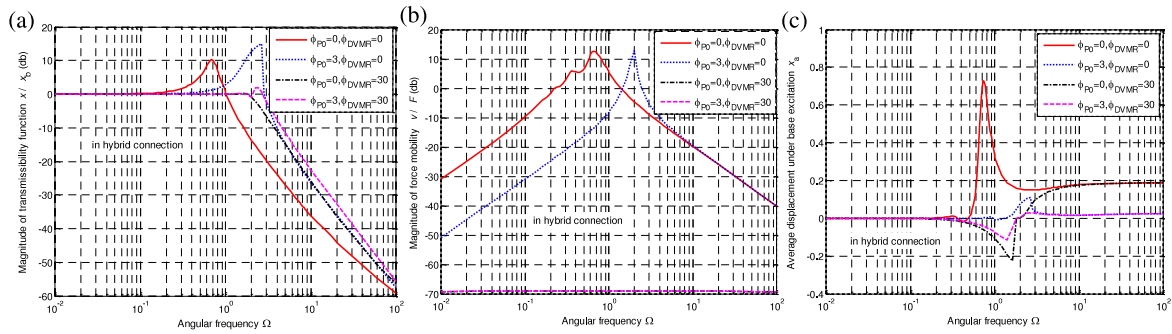


Figure 17. Performance of the MrEPI under adjustable additional pressure ratio ϕ_{P0} and MR active damping ϕ_{DVMR} . (a) Generalized transmissibility under base excitation. (b) Force mobility function under force excitation. (c) Average displacement under base excitation.

Table 1. Performance evaluation under additional volume ratio and dynamic range of MR active damping.

(a) Performance comparison under base excitation							
Low stiffness				High stiffness			
		Resonant frequency	Peak value (db)	Maximum average displacement near resonant frequency	Resonant frequency	Peak value (db)	Maximum average displacement near resonant frequency
Hybrid connection	Low damping	0.4	11.0106	0.2815	0.68	10.2622	0.7296
	High damping		0.1298	-0.2494		0.1180	-0.2271
Parallel connection	Low damping	0.4	12.7057	0.3262	0.66	15.1707	1.9492
	High damping		0.1166	-0.2302		0.1311	-0.2302
Series connection	Low damping	0.4	4.4508	0.1347	0.68	13.2029	1.3663
	High damping		2.8794	0.0480		6.7423	0.5198

(b) Performance comparison under force excitation							
Low stiffness				High stiffness			
		Magnitude of force mobility at $\Omega = 0.01$ (db)	Maximum average displacement near resonant frequency	Magnitude of force mobility under $\Omega = 0.01$ (db)	Maximum average displacement near resonant frequency		
Hybrid connection	Low damping	-21.4179	8.3047	-30.9740	2.7959		
	High damping	-69.2498	0.0021	-69.2635	0.0020		
Parallel connection	Low damping	-21.4183	9.8903	-30.9736	8.6032		
	High damping	-69.2511	0.0021	-69.2623	0.0020		
Series connection	Low damping	-21.4147	2.7019	-30.9736	6.1401		
	High damping	-22.9929	2.0537	-36.9747	0.5476		

4.5.2. Achievable performance through adjusting the additional pressure and MR active damping. Figure 17 shows the effects of the additional pressure ratio ϕ_{P0} and MR active damping ϕ_{DVMR} , where ϕ_{P0} is used to adjust the stiffness and ϕ_{DVMR} is used to adjust the damping. The performance evaluation is given in table 2 with comparisons with the corresponding performances for parallel and series connections, which indicate that the hybrid structure is much better than the others in terms of the achievable stiffness and peak values. In figure 17(a), the system resonance frequency could be changed over a large range from 0.68 to 2.6 by adjusting ϕ_{P0} (larger ϕ_{P0} results in a larger resonance frequency and the stiffness could be set for different requirements). Also, from figures 17(a) and (b) the transmissibility peak and force mobility magnitude could be decreased obviously with a larger damping while the decaying rate at high frequency was retained (no matter whether with low stiffness or high stiffness). The unsatisfactory nonlinear

characteristics (multiple peaks and large average displacement around resonance frequency) can all be mitigated (figure 17).

Therefore, similarly to the cases of adjusting the additional air volume, the isolation performance including a smaller peak value and better capability in force mobility as well as minimum average displacement around the resonance frequency could all be achieved due to the independently adjustable stiffness and damping. The height of the isolator can be adjusted through pressure regulation (see section 4.2).

5. Conclusions

A new vibration isolator MrEPI is proposed and systematically analyzed, which can provide independently adjustable stiffness and damping characteristics, and is able to work in different (passive/semi-active/active) control modes. A systematic nonlinear non-dimensional analysis of the MrEPI is conducted by considering the linear and nonlinear components involved

Table 2. Performance evaluation under additional pressure ratio and dynamic range of MR active damping.

(a) Performance comparison under base excitation							
		Low stiffness			High stiffness		
		Resonant frequency	Peak value	Maximum average displacement near resonance frequency	Peak value	Resonance frequency	Maximum average displacement near resonance frequency
Hybrid connection	Low damping	0.6800	10.2623	0.7295	14.8810	2.6000	0.1108
	High damping		0.1293	-0.2271	1.8913		-0.1143
Parallel connection	Low damping	0.66	15.1707	1.9492	15.0053	2.6	0.1108
	High damping		0.1311	-0.2302	11.5207		-0.1170
Series connection	Low damping	0.6800	13.2029	1.3663	15.7909	0.7600	3.1007
	High damping		6.7385	0.5198	3.7008		0.1848

(b) Performance comparison under force excitation							
		Low stiffness			High stiffness		
		Magnitude of force mobility at $\Omega = 0.01$		Maximum average displacement near resonant frequency	Magnitude of force mobility at $\Omega = 0.01$		Maximum average displacement near resonant frequency
Hybrid connection	Low damping	-30.9740		2.7959	-50.7963		0.0423
	High damping	-69.2635		0.0020	-69.4262		0.0012
Parallel connection	Low damping	-30.974		8.6032	-50.6809		0.0553
	High damping	-69.2623		0.0020	-69.4245		0.0012
Series connection	Low damping	-30.9736		6.1401	-36.3360		5.6242
	High damping	-36.9747		0.5476	-56.4237		-0.0386

in the pneumatic springs and MR dampers subject to harmonic excitation. The present study not only demonstrates a clear insight into the advantageous dynamic performance of the proposed MrEPI, but also provides a systematic non-dimensional model for the analysis and design of nonlinear vibration isolators with pneumatic springs and MR dampers. The MrEPI has the following dynamic characteristics.

- (1) The nonlinearity degree of the pneumatic spring element is strongly dependent on the initial length of the pneumatic chamber and the excitation amplitude. The nonlinear characteristics of the pneumatic spring such as superharmonics in transmissibility, subharmonics in force mobility and large average displacement around the resonance frequency can all be obviously weakened through utilizing the auxiliary chamber and restrictor connecting to the working chamber under small volume constraint.
- (2) The stiffness of the MrEPI could be designed or controlled purposely with invariant static displacement either by appropriately changing the additional pressure ratio (i.e., the difference between the additional pressure and the reference pressure) and the pressure ratio of the dual-working-chamber pneumatic spring simultaneously, or by changing the additional volume ratio (i.e., the difference between the additional volume and the reference volume). The pressure control is functionally equivalent to control of the volume at different static displacements under the same static load for a single-working-chamber pneumatic spring case. The height control can be achieved through pressure regulation of two working chambers regardless of pressure balance for certain payloads.
- (3) The nonlinear dynamic characteristics of the MR active damping in the MrEPI demonstrate noticeable advantages for the attenuation of resonance peaks and maintenance of a fast decaying rate at high frequency compared to the corresponding linear viscous damping. Furthermore, the magnitude of the force mobility is decreased significantly and kept nearly constant at all frequencies when the nonlinear MR damping is set larger, which could be used to effectively improve the performance of resisting force disturbance. In addition, the effective MR damping can also be controlled by choosing properly the hysteretic width coefficient or the hysteretic slope coefficient.
- (4) The proposed MrEPI, which employs a hybrid configuration of two pneumatic elements in series connection and one MR damping element in parallel connection, exhibits excellent and flexible isolation performance (e.g., small resonance peak values and high capability of resisting force disturbance as well as fast decaying rate at high frequencies under certain stiffnesses) because of the independently adjustable stiffness and damping characteristics.

Acknowledgments

The authors gratefully acknowledge the constructive comments and suggestions from the reviewers, and also support from the GRF project (Ref 517810) of Hong Kong RGC, Department General Research Funds and Competitive Research Grants of Hong Kong Polytechnic University.

Appendix

Table A.1. Default values and illustrations of non-dimensional variables for the MrEPI.

Variable	Name	Default Value	Illustration
ϕ_L	Nonlinearity degree ratio	5	Ratio of reference initial length of pneumatic spring to excitation amplitude
λ	Polytropic exponent	1.4	Parameter influencing the heat process
ϕ_{P0}	Additional pressure ratio	0	Ratio of additional initial pressure to reference pressure
ϕ_{V0}	Additional volume ratio	0	Ratio of additional initial volume to reference volume
ϕ_{KP}	Pressure ratio of dual-working-chamber pneumatic spring	0	Ratio of pressure of upper pneumatic chamber to reference pressure
ϕ_{KL}	Volume ratio of dual-working-chamber pneumatic spring	1	Ratio of initial length of upper pneumatic chamber to reference length
ξ	Passive viscous damping	0.05	Passive linear viscous damping
ϕ_{DVMR}	Dynamic range of MR active damping	0	Dynamic range of active damping due to field-controlled yield force of MR fluid
$\phi_{\lambda 1}$	Hysteretic width coefficient	0.001	Parameter to capture the displacement-dependent hysteresis width in the MR damping model
$\phi_{\lambda 2}$	Hysteretic slope coefficient	1000	Parameter to capture the velocity-dependent hysteresis slope in the MR damping model
r_F	Unified coefficient for base and force excitation	1	Unifying the non-dimensional variables for force excitation and base excitation
ξ_3	Viscous damping of the restrictor	1000	Passive damping of auxiliary chamber (large damping functions as a block for the two pneumatic chambers)

Table A.2. Illustrations of symbols for the MrEPI.

Symbol	Illustration	Symbol	Illustration
P	Absolute gas pressure (bar)	V	Gas volume (m ³)
A	Effective area of pneumatic chamber (m ²)	L	Length of pneumatic chamber (m)
T	Temperature of pneumatic chamber (K)	m_a	Air mass in pneumatic chamber (kg)
d_c, l_c	Diameter and length of the capillary tube as an air restrictor, respectively (m)	Q_m	Air mass flow rate through valve of capillary tube (kg s ⁻¹)
μ	Dynamic viscosity of air (Pa s)	ρ	Density of air (kg m ⁻³)
F_s	Output force of pneumatic spring element (N)	F_d	Output force of MR damping element (N)
F_{sa}	Output force of pneumatic spring element due to upper chamber (N)	F_{sb}	Output force of pneumatic spring element due to low chamber (N)
F_{da}	Active damping force of MR damping element (N)	F_{dp}	Passive damping force of MR damping element (N)
K_a, K_b, K_c	Linearized stiffness due to upper chamber, low chamber and auxiliary chamber, respectively (N m ⁻¹)	K	Linearized stiffness (N m ⁻¹)
m	Payload mass (kg)	R	Gas constant of air (J kg ⁻¹ K ⁻¹)
k_0	Reference stiffness (N m ⁻¹)	L_0	Initial length of pneumatic spring (L)
λ	Polytropic exponent	V_M	Maximum velocity of the isolator (m s ⁻¹)
c_{vis}, c_a	Viscous damping coefficient and equivalent active damping coefficient, respectively (N s m ⁻¹)	ξ, ξ_a	Viscous damping ratio and equivalent active damping ratio, respectively
\hat{x}_{b0}	Displacement amplitude under sinusoidal excitation (m)	\hat{F}_0	Force amplitude under sinusoidal excitation (N)
λ_1	Scale factor that captures the shape of the displacement-dependent hysteresis loop in the MR damping model (s ⁻¹)	λ_2	Scale factor that captures the hysteresis slope of the yield force in the MR damping model (s m ⁻¹)
x	Absolute displacement of payload (m)	ω	Excitation frequency (rad s ⁻¹)
t	Excitation time (s)	η	Viscosity of MR fluid (Pa s)
r_m, r_r	Radius of piston and radius of piston rod in MR fluid cylinder, respectively (m)	w, d, r_d	Circumference of the annulus, gap size of the annulus, inner radius of the annulus of the MR valve (m)
l_a, l_p	Gap lengths in the active and passive domains of the MR valve, respectively (m)	r_t, l_t	Radius and total length of the circular tubing, respectively (m)
H	Applied magnetic field intensity (A m ⁻¹)	F_f	Friction force due to shaft seals (N)
f_c	Coefficient that depends on the flow velocity profile in the MR valve and range at [2.07, 3.07]	τ_y	Dynamic yield shear stress of MR fluid (Pa)
s_u	Switching flag with $s_u = 0$ for the case of a single-working-chamber pneumatic spring (i.e. the relative pressure of the upper chamber of the pneumatic spring is zero), and $s_u = 1$ for the case of the double-working-chamber pneumatic spring		

Table A.3. Illustrations of subscripts and prefixes for symbols.

Subscript	Illustration	Subscript	Illustration
0	Static or initial value	n	Non-dimensional output
u	Upper chamber	b	Motion for base excitation
d	Low chamber	m	Motion for middle plate of an isolator
c	Auxiliary chamber	r	Reference state
atm	Atmosphere		
$i = 1, 2, 3$	Component consisting of pneumatic spring and MR damping element		
Prefix	Illustration	Prefix	Illustration
Δ	Variation of variables	ϕ	Non-dimensional variable

References

- [1] Piersol A G and Paez T L 2010 *Shock and Vibration Handbook* 6th edn (New York: McGraw-Hill)
- [2] Fundamentals-vibration-isolation <http://www.cvimellesgriot.com/Products/Documents/Technical-Guide/Fundamentals-Vibration-Isolation.pdf>
- [3] Choi Y T and Wereley N M 2005 Semi-active vibration isolation using magnetorheological isolators *J. Aircraft* **42** 1244–51
- [4] Mizuno T, Takasaki M and Murashita M 2005 *Pneumatic Zero-compliance Mechanism Using Negative Stiffness, IUTAM Symp. on Vibration Control of Nonlinear Mechanisms and Structures Solid Mechanics and Its Applications* vol 130, pp 213–22
- [5] Eslaminasa N, Vahid O A and Golnaraghi F 2010 Nonlinear analysis of switched semi-active controlled systems *Veh. Syst. Dyn.* **49** 291–309
- [6] Ebrahimi B 2009 Development of hybrid electromagnetic dampers for vehicle suspension systems *DEng Thesis* University of Waterloo, Waterloo, Canada
- [7] Yan T H, Pu H Y, Chen X D, Li Q and Xu C 2010 Integrated hybrid vibration isolator with feedforward compensation for fast high-precision positioning X/Y tables *Meas. Sci. Technol.* **21** 65901–10
- [8] Nitta M and Hashimoto S 2008 Identification and control of precision XY stages with active vibration suppression system *13th Power Electronics and Motion Control Conference (Poznan 2008)* pp 932–7
- [9] Hoque M E, Takasaki M, Ishino Y, Suzuki H and Mizuno T 2006 An active micro vibration isolator with zero-power controlled magnetic suspension technology *JSME Int. J. C* **29** 719–26
- [10] Batterbee D C and Sims N D 2005 Vibration isolation with smart fluid dampers: a benchmarking study *Smart Struct. Syst.* **1** 235–56
- [11] Baudry M, Micheau P and Berry A 2006 Decentralized harmonic active vibration control of a flexible plate using piezoelectric actuator–sensor pairs *J. Acoust. Soc. Am.* **119** 262–77
- [12] Marouze J P and Cheng L 2002 A feasibility study of active vibration isolation using THUNDER actuators *Smart Mater. Struct.* **11** 854–62
- [13] Fanucci J P 2008 Shape memory alloy composite material shock and vibration isolator devices *US Patent App.* 12/080,090
- [14] Ribakov Y 2009 Semi-active pneumatic devices for control of MDOF structures *Open Construct. Build. Technol. J.* **3** 141–5
- [15] Lee J H and Kim K J 2007 Modeling of nonlinear complex stiffness of dual-chamber pneumatic spring for precision vibration isolations *J. Sound Vib.* **301** 909–26
- [16] Nieto A J, Morales A L, Gonzalez A, Chicharro J M and Pintado P 2008 An analytical model of pneumatic suspensions based on an experimental characterization *J. Sound Vib.* **313** 290–307
- [17] Porumamilla H 2007 Modeling, analysis and non-linear control of a novel pneumatic semi-active vibration isolator: a concept validation study *DEng Thesis* Iowa State University, USA
- [18] Deo H V 2007 Axiomatic design of customizable automotive suspension systems *DEng Thesis* Massachusetts Institute of Technology, USA
- [19] Fei H Z, Zheng G T and Liu Z G 2006 An investigation into active vibration isolation based on predictive control part I *J. Sound Vib.* **296** 195–208
- [20] Shih M C and Wang T Y 2008 Active control of electro-rheological fluid embedded pneumatic vibration isolator *Integr. Comput.-Aided Eng.* **15** 267–76
- [21] Maciejewski I 2010 Modelling and control of semi-active seat suspension with magneto-rheological damper *XXIV Symp. Vibrations in Physical Systems (Poznan–Bedlewo, May 2010)*
- [22] Kim H, Lee K, Kim C, Lee G and Son S 2009 An electro-magneto-pneumatic spring for vibration control in semiconductor manufacturing *Proc. IEEE Int. Conf. on Mechatron (Malaga)* pp 1–6
- [23] Fowler L P, Buchner S and Ryaboy V 2000 Self-contained active damping system for pneumatic isolation tables *Industrial and Commercial Applications of Smart Structures, Technologies (Newport Beach, March 2000)* pp 261–72
- [24] Tanner E T 2003 Combined shock and vibration isolation through the self-powered, semi-active control of a MR damper in parallel with an air spring *PhD Thesis* Virginia Polytechnic Institute and State University
- [25] Spelta C, Previdi F, Savaresi S M, Bolzern P, Cutini M and Bisaglia C 2010 A novel control strategy for semi-active suspensions with variable damping and stiffness *American Control Conference (Baltimore, June–July 2010)* pp 4582–7
- [26] Liu Y, Matsuhsa H and Utsuno H 2008 Semi-active vibration isolation system with variable stiffness and damping control *J. Sound Vib.* **313** 16–28
- [27] Wang D H and Liao W H 2011 Magnetorheological fluid dampers: a review of parametric modelling *Smart Mater. Struct.* **20** 023001
- [28] Yang G, Spencer B F, Carlson J D and Sain M K 2002 Large-scale MR fluid dampers: modeling, and dynamic performance considerations *Eng. Struct.* **24** 309–23
- [29] Muhammad A, Yao X and Deng Z 2006 Review of magnetorheological (MR) fluids and its applications in vibration control *Eng. J. Mar. Sci. Appl.* **5** 17–29
- [30] Nam Y J and Park M K 2007 Performance evaluation of two different bypass-type MR shock dampers *J. Intell. Mater. Syst. Struct.* **18** 707–17
- [31] Hong S R, Wang G, Hu W and Wereley N M 2006 Liquid spring shock absorber with controllable magnetorheological damping. Proceedings of the institution of mechanical engineers, part D *J. Automobile Eng.* **220** 1019–29

- [32] Duan Y F, Ni Y Q and Ko J M 2006 Cable vibration control using magnetorheological dampers *J. Intell. Mater. Syst. Struct.* **17** 321–5
- [33] Choi Y T and Wereley N M 2009 Self-powered MR dampers *J. Vib. Acoust.* **131** 044501
- [34] Hong S R, Choi S B, Choi Y T and Wereley N M 2005 Non-dimensional analysis and design of a magnetorheological damper *J. Sound Vib.* **288** 847–63
- [35] Facey W B, Rosenfeld N C, Chois Y T and Wereley N M 2005 Design and testing of a compact MR damper for high impulsive loads *Int. J. Mod. Phys. B* **19** 1549–55
- [36] Li W H, Wang X Y, Zhang X Z and Zhou Y 2009 Development and analysis of a variable stiffness damper using an MR bladder *Smart Mater. Struct.* **18** 074007
- [37] Achen A, Toscano J, Marjoram R, Stclair K, McMahan B, Goelz A and Shutto S 2008 Semi-active vehicle cab suspension using magnetorheological (MR) technology *Proc. 7th JFPS Int. Symp. on Fluid Power (Toyama, Sept. 2008)* pp 561–4
- [38] Liu Y, Matsuhisa H, Utsuno H and Park J G 2006 Vibration control by a variable damping and stiffness system with magnetorheological dampers *JSME Int. J. C* **49** 411–7
- [39] Heertjes M F and van de Wouw N 2006 Nonlinear dynamics and control of a pneumatic vibration isolator *J. Vib. Acoust.* **128** 439–48
- [40] Nieto A J, Morales A L, Trapero J R, Chicharro J M and Pintado P 2011 An adaptive pneumatic suspension based on the estimation of the excitation frequency *J. Sound Vib.* **330** 1891–903
- [41] Zhong Y C, Yang Q J and Bao G 2010 Nonlinearity analyses of pneumatic vibration isolation system with simple harmonic excitations *ICCSIT: 3rd IEEE Int. Conf. on Computer Science and Information Technology (Chengdu, July 2010)* pp 814–7
- [42] Liao W H and Lai C Y 2002 Harmonic analysis of a magnetorheological damper for vibration control *Smart Mater. Struct.* **11** 288–96
- [43] Snyder R A, Kamath G M and Wereley N M 2001 Characterization and analysis of magnetorheological damper behavior under sinusoidal loading *AIAA J.* **39** 1240–53
- [44] Hong S R, Wereley N M, Choi Y T and Choi S B 2008 Analytical and experimental validation of a nondimensional bingham model for mixed-mode magnetorheological dampers *J. Sound Vib.* **312** 399–417
- [45] Quaglia G and Sorli M 2001 Air suspension dimensionless analysis and design procedure *Veh. Syst. Dyn.* **35** 443–75
- [46] Liu Y, Waters T P and Brennan M J 2005 A comparison of semi-active damping control strategies for vibration isolation of harmonic disturbances *J. Sound Vib.* **280** 21–39
- [47] Iyengar V R, Alexandridis A A, Tungb S C and Ruleb D S 2004 Wear testing of seals in magneto-rheological fluids *Tribol. Trans.* **47** 23–8
- [48] Carlson J D and Jolly M R 2000 MR fluid foam and elastomer devices *Mechatronics* **10** 555–69
- [49] Kordonski W I and Gorodkin S R 1996 Magnetorheological fluid-based seal *J. Intell. Mater. Syst. Struct.* **7** 569–72
- [50] Jolly M R, Bender J W and Carlson J D 1999 Properties and applications of commercial magnetorheological fluids *J. Intell. Mater. Syst. Struct.* **10** 5–13
- [51] Al-Dakkan K A, Barth E J and Goldfarb M 2006 Dynamic constraint-based energy-saving control of pneumatic servo systems *J. Dyn. Syst., Meas. Control* **128** 655–62
- [52] Zhu X C, Tao G L, Yao B and Cao J 2008 Adaptive robust posture control of a parallel manipulator driven by pneumatic muscles *Automatica* **44** 2248–57
- [53] Mao M, Hu W, Choi Y T and Wereley N M 2007 A magnetorheological damper with bifold valves for shock and vibration mitigation *J. Intell. Mater. Syst. Struct.* **18** 1227–32
- [54] Dunn D J *Applied Fluid Mechanics Tutorial No.6 Dimensional Analysis, Applied Fluid Mechanics Solution—eBook* <http://www.freestudy.co.uk/fluid%20mechanics/t6203.pdf>
- [55] Ibrahim R A 2008 Recent advances in nonlinear passive vibration isolators *J. Sound Vib.* **314** 371–452
- [56] Jing X J, Lang Z Q and Billings S A 2008 Frequency domain analysis for suppression of output vibration from periodic disturbance using nonlinearities *J. Sound Vib.* **314** 536–57